A comparative evaluation of three hydrophones and a numerical model in high intensity focused ultrasound fields

Julian Haller and Klaus-Vitold Jenderka
Physikalisch-Technische Bundesanstalt, Bundesallee 100, 38116 Braunschweig, Germany

Gianni Durando
Istituto Nazionale Di Ricerca Metrologica, Strada delle Cacce 91, 10135 Turin, Italy

Adam Shaw
National Physical Laboratory, Teddington, Middlesex, TW11 0LW, United Kingdom

(Received 6 June 2011; revised 5 December 2011; accepted 7 December 2011)

The pressure fields of two different high intensity focused ultrasound (HIFU) transducers operated in burst mode were measured at acoustical power levels of 25 and 50 W (continuous wave equivalent) with three different hydrophones: A fiber-optic displacement sensor, a commercial HIFU needle hydrophone, and a prototype of a membrane hydrophone with a protective coating against cavitation effects. Additionally, the fields were modeled using a freely available simulations software package. The measured waveforms, the peak pressure profiles, as well as the spatial-peak temporal-average intensities from the different devices and from the modeling are compared and possible reasons for differences are discussed. The results clearly show that reliable pressure measurements in HIFU fields remain a difficult task concerning both the reliability of the measured values and the robustness of the sensors used: Only the fiber-optic hydrophone survived all four exposure regimes and the measured spatial-peak temporal-average intensities varied by a factor of up to 1.5 between the measurements and the modeling and between the measurements among themselves. © *2012 Acoustical Society of America*. [DOI: 10.1121/1.3675003]

PACS number(s): 43.35.Yb, 43.80.Vj [TDM] Pages: 1121–1130

I. INTRODUCTION

High intensity focused ultrasound (HIFU) is a noninvasive therapy technique, where ultrasound is focused in a small elliptical volume (diameter ≈ 1 mm, length ≈ 1 cm).[1–5] Due to sound absorption, the tissue within this volume is rapidly heated and necrotized. Owing to its noninvasive character and its claimed minor side effects, the number of HIFU treatments of tumors has been growing during the past few years and several different HIFU applications have been developed.[6–10] The prerequisite of successful treatment with as few side effects as possible is an accurate treatment planning to achieve complete necrosis inside the intended treatment area and to prevent necrosis outside of it. This requires a good knowledge of the sound field of the ultrasonic transducer used.

Conventional sensors for sound field characterization generally cannot endure the extreme conditions in the focus of a HIFU field. Hence, several attempts have been made to develop sensors with adequate robustness and temporal and spatial resolution for measurements in HIFU fields. One strategy is to modify well-known piezoelectric devices, primarily to improve their robustness. For example, a needle hydrophone with a metallic coating above the sensing element was presented recently.[11] Another promising strategy is the development of small and robust fiber-optic probes that use an acousto-optic effect at their end face to measure the pressure or the displacement in HIFU fields.[12–16] Some other methods avoid putting a sensor in the focal region: Methods have been presented,[17,18] where a reflective scattering element is exposed to the focus instead of the sensor itself and sensitive elements measure the scattered sound field. Finally, some different methods are presented that work noninvasively by monitoring the particle displacement in a HIFU field, e.g., with magnetic resonance imaging,[19] particle image velocimetry (PIV),[20] or schlieren imaging.[21] However, these noninvasive methods are not yet suitable for quantitative measurements, because they are difficult to calibrate and some of them provide only two-dimensional projection images of sound fields.

For all these devices, the challenge besides the robustness requirements is the correct determination of the desired quantities (typically the temporal behavior of the pressure or the particle displacement) from the acquired transient voltages. The two common strategies to achieve this are either to perform a calibration to determine the transfer function of the device or to compare measurement results from the device with those from a reference, such as a membrane hydrophone. However, both the calibration and the comparison have to be performed in fields that are considerably weaker than HIFU fields to not destroy the reference or the standard. It remains debatable whether the suitability of a measuring device, which has been proven only in a weak plane wave ultrasound field, can also be assumed in HIFU fields. Thus, in the present paper, we investigate whether different sensors yield the same results in the fields of strongly focusing HIFU transducers at practical power levels as well.

The field of a HIFU transducer can also be predicted using computer simulations,[16,22–26] which are usually based

on the solution of the Khokhlov–Zabolotskaya–Kuznetsov (KZK) equation,[27] which includes nonlinear propagation effects. Some of the simulations use only nominal parameters of the transducer (aperture, active diameter, fundamental frequency, etc.) as input data, which of course does not take into account any imperfections in the transducer. Other simulations make use of the sound field measured at low drive voltage or close to the transducer as input data for a forward calculation to the focal region. Numerical algorithms using the KZK equation have been applied to a variety of medical ultrasonic fields including HIFU[16,28–30] and, generally, good agreement of results from modeling with measurements has been observed around the focal region.

In this paper we present and compare the results of hydrophone measurement and computer simulations for two transducers at peak-to-peak pressures up to ~40 MPa. The hydrophones used were an in-house fiber-optic device from the Physikalisch-Technische Bundesanstalt (PTB), a prototype membrane hydrophone with a polyurethane coating, and a commercially available needle hydrophone intended for HIFU use (HNA-0400, ONDA Corp., Sunnyvale, CA). The computer simulation is a freely available MATLAB package to solve the KZK equation [HIFU-Simulator v1.0, Food and Drug Administration (FDA), Silver Spring, MD). The purpose of this study was to examine whether the results from different devices are in good agreement for a practical measurement situation. The measurements were carried out at PTB, and the work was part of a much larger European project called "External Beam Cancer Therapy."[31]

II. DEVICES AND METHODS

A. Fiber-optic displacement sensor

The fiber-optic displacement sensor with a heterodyne interferometric setup, which was used in this work, has been described previously.[16] The sensor is a single-mode fiber with an outer diameter of 125 μm, which has been titanium-coated (thickness 200 nm) to provide an optically reflecting end surface. This fiber tip forms the end of the measuring arm of a heterodyne interferometer. An incoming sound wave causes a change in the optical path length of this arm and, thus, a phase modulation of the reflected light. This phase modulation is then measured and analyzed by a heterodyne interferometer and a delay line discriminator. It must be noted that this sensor measures the particle displacement ξ instead of the pressure p. While in a plane wave, these values are related as

$$p(t) = \rho \cdot c_s \cdot \frac{\partial \xi}{\partial t}, \tag{1}$$

with the density of the medium, ρ, and the speed of sound, c_S, it is not absolutely certain whether Eq. (1) is valid without limitations in strongly focused nonlinear HIFU fields.

Nevertheless, the frequency dependence of the complex transfer function (defined as the ratio of the instantaneous end-of-cable voltage to the instantaneous acoustical pressure) of the present sensor was calibrated in compliance with an established calibration procedure[32] at PTB from 0.48 to 250 MHz in steps of 0.12 MHz. For the present study, the output of the device was lowpass-filtered to reduce high frequency noise using a third-order Butterworth filter with a −3 dB cutoff frequency $f_G = 100$ MHz. In Fig. 1, the magnitude and the phase of the frequency response of the device are shown to 40 MHz along with those of the other two devices as far as available, and in Table I some general characteristics of the devices are listed.

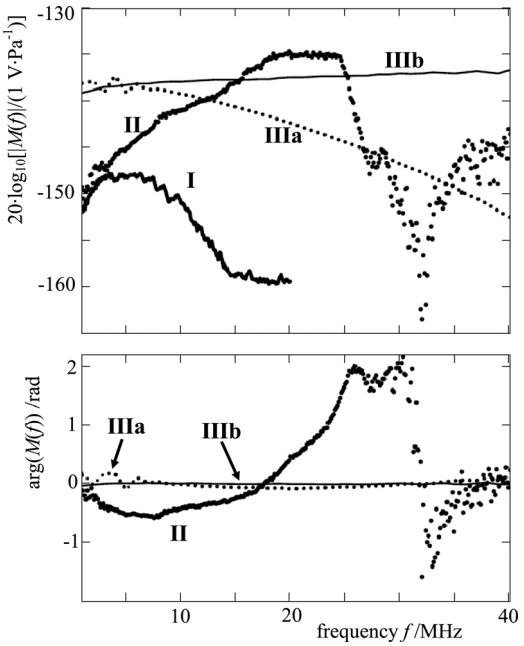

FIG. 1. Magnitude (top) and phase (bottom) frequency response data of the employed three HIFU sensors. I: Needle hydrophone HNA-0400; II: Fiber-optic displacement sensor (data for $f > 40$ MHz not shown); III: Membrane hydrophone with (IIIa) and without (IIIb) PU-coating. The magnitude data for the fiber-optic probe and the membrane hydrophone have been shifted upward by 40 and 20 dB, respectively, so that all data can fit in the same scale.

B. Needle hydrophone ONDA HNA-0400

One of the very few commercially available HIFU hydrophones is the HNA-0400 from ONDA Corporation. It consists of a sensing piezoceramic element with a diameter of 400 μm, which is protected by a metallic coating with a thickness between 20 and 70 μm.[11] The amplitude of the frequency response, as well as the capacitance $C_H(f)$ of the hydrophone, were supplied by the manufacturer from 1 to 20 MHz in steps of 50 kHz. As an additional cable had to be used between the hydrophone and the oscilloscope, the given frequency response M_0 was corrected with the following formula:[33]

TABLE I. Comparison of some relevant parameters of the three hydrophones. The term usable bandwidth denotes either the calibrated frequency range or in the case of the fiber-optic sensor the considered frequency range.

Parameter	Fiber-optic setup	ONDA HNA-0400	Coated membrane
Sensor form	Fiber	Needle	Membrane
Measured value	Displacement	Pressure	Pressure
Sensing diameter (μm)	125	400	200
Usable bandwidth (MHz)	100	20	40

$$M(f) = M_0(f) \cdot \frac{C_H(f)}{C_H(f) + C_C}, \quad (2)$$

where the capacitance of the cable, $C_C = 154$ pF, was taken from the specification of the cable ($C/l = 100$ pF/m, type RG-58 C/U). The capacitance of the hydrophone according to the manufacturer decreases from 113 pF at 1 MHz to 45 pF at 20 MHz. Hence, the correction in Eq. (2) has a rather large influence on the frequency response and, in general, the use of a preamplifier would be advisable.

C. Coated membrane hydrophone

To the authors' knowledge, there are no membrane hydrophones commercially available that are suitable for use in HIFU fields. However, membrane hydrophones that withstand peak compressional pressure values of ~27 MPa have been reported,[34] and the linearity of polyvinylidene fluoride (PVDF) has been demonstrated up to higher levels using specially designed PVDF hydrophones for underwater acoustic applications:[35,36] Negligible changes, within 0.6 dB, in the frequency response of the hydrophones were observed up to hydrostatic pressures of 69 MPa. If there is a weakness already present, damage can be caused at high negative pressures by delamination of bilaminar hydrophones. A more common cause of damage is loss of the metal electrodes due to cavitation in the water immediately in front of or behind the hydrophone. In order to protect the vulnerable electrodes, a coplanar membrane hydrophone 12 μm in thickness with a 0.2 mm nominal diameter active element (C1202 with integrated preamplifier, Precision Acoustics, Dorchester, UK) was coated with a polyurethane layer on both sides. The coating was originally designed as an impedance matching layer and has the same composition as the clear layer of the HAM-A radiation force balance target[37] at the National Physical Laboratory (NPL). At 20 °C, the speed of sound in the material was measured to be 1580 m s^{-1} at 1 MHz and 1588 m s^{-1} at 3 MHz, the absorption coefficient was 4 dB cm^{-1} MHz$^{-1.46}$ between 1 and 5 MHz, and the reflection coefficient was –45 dB at 1 MHz and −40 dB at 3 MHz. Both sides of the hydrophone were spray-coated to a thickness of approximately 0.4 mm. The device was calibrated before and after coating at NPL using a nonlinear comparison method, which gave the frequency response from 1 to 40 MHz in steps of 1 MHz. The magnitude and phase response before and after coating are shown in Fig. 1. In comparison to the uncoated response, the coating process has introduced ripples in both the magnitude and phase responses of the hydrophone below 10 MHz, and has significantly reduced the magnitude for higher frequencies. However, the −6 dB bandwidth is ~30 MHz, and the phase response is flat to within ±0.15 rad up to 40 MHz. The use of thinner coating layers would increase the frequency of the ripples and reduce the drop off at high frequencies.

D. HIFU-Simulator

Simulations were performed with the HIFU-Simulator, which is a freely distributed MATLAB-based software package.[22] The propagation module of this software solves the KZK equation using a split-step method. Within each step, first the linear parts of the KZK equation are computed in the frequency domain and then the nonlinear parts are computed in the time domain. As input data for the software transducer parameters, medium properties (in this study, water) and computational parameters are needed: Transducer parameters (radius a_{act}, focusing depth z_{foc}, fundamental frequency f_0, acoustical power P_{ac}) are listed in Table II as given by the manufacturer. Water properties were assumed to be: Speed of sound $c_S = 1482$ m/s, density $\rho = 10^3$ kg/m^3, ultrasound absorption at 1 MHz $\alpha_{1MHz} = 0.217$ dB/m, exponent of absorption vs frequency $\eta_1 = 2$, and nonlinearity parameter $\beta = 3.5$. Computational parameters were: Radius of the computational domain $R = a_{act}$, length of the computational domain $Z = 2z_{foc}$, and number of considered harmonics $K = 100$. Besides data considering thermal aspects, the peak compressional pressure values p_c, the peak rarefactional pressure values p_r, the intensity I, as well as the pressure waveform $p(t)$ at the focus are available as output data. The amplitude of the acoustic pressure is calculated from the acoustic output power on the assumption that the amplitude at distance $z = 0$ is uniform over a flat disk of radius a_{act} and zero outside this radius; the phase distribution over the disk surface was calculated to give a circular wavefront converging on the center of curvature.

Due to the parabolic approximation of the KZK equation, the claimed validity of the simulation software is limited to transducers with an f-number larger than 1.37. Only one of the transducers meets this criterion (see the next section), but the calculations were performed for both transducers to test the validity of the simulations for smaller f-numbers.

E. Experimental setup

All measurements were performed in the same experimental setup at PTB. Two different transducers were used: SU-101 and H-108MRA (Sonic Concepts, Bothell, WA). Both transducers were equipped with external matching networks. Some relevant parameters of the transducers are listed in Table II. HIFU driving signals were generated with an arbitrary function generator (Model AFG3101, Tektronix, Beaverton, OR) and were amplified with a 500 W power amplifier (Model 500A100A, Amplifier Research, Souderton, PA). The generated signals were tone bursts of 20 cycles duration at the fundamental frequency of the transducer used and the pulse repetition rate was 1 kHz. The hydrophone voltage signals were monitored and measured with a digital phosphor oscilloscope (Tektronix DPO7104, 500 MHz bandwidth, 500 MS/s data acquisition) with input impedance set to 1 MΩ for the HNA-0400 and 50 Ω for the membrane

TABLE II. Some relevant parameters of the employed HIFU transducers. Fundamental frequency f_0, focusing depth z_{foc}, active radius a_{act}, f-number $F(=z_{foc}/2a_{act})$, electro-acoustic efficiency P_{ac}/P_{el}, and on-time of the tone burst τ_{on}.

Transducer	f_0 (MHz)	z_{foc} (mm)	a_{act} (mm)	F	P_{ac}/P_{el}	τ_{on} (μs)
SU-101	1.98	55	17.5	1.57	0.885	10.1
H-108MRA	2.45	50	30	0.83	0.545	8.2

hydrophone and the fiber-optic hydrophone. A standard PC workstation with an in-house Delphi software was used to acquire the data from the oscilloscope and to control the positioning system (in-house setup).

Each transducer/power level/hydrophone combination was considered as one measurement unit and one measurement unit was performed per day. The measuring procedure for each measurement unit was as follows: The measurement tank was filled with freshly degassed (oxygen content as measured by chance: < 2 mg/l), de-ionized and distilled water and the transducer and hydrophone were immersed in that tank for 1 h. Then the desired power level was adjusted by varying the output voltage of a continuous wave signal of the function generator and by measuring the electrical output power level behind the amplifier with a power level meter (Model NRT with sensor head NAP Z-8, Rohde & Schwarz, Munich, Germany). The corresponding acoustic power was calculated from the electro-acoustic efficiency P_{ac}/P_{el}, which had been measured before with a radiation force balance for both transducers. Afterward, the hydrophone was roughly brought into the focal region and the tone burst signal with the same amplitude was switched on. The given power levels thus do not belong to the burst mode signals investigated, but to continuous wave signals with the same driving voltage amplitude instead. Then the exact focal position was sought by finding the position where the hydrophone signal (peak-to-peak) had its absolute maximum, and the automatic scanning procedures were started. Three scans were carried out: An axial scan along the z axis and a pair of orthogonal radial scans along the x and y axes through the focus. During these scans, the hydrophone was moved from the starting position to the end position in steps of 0.1 mm and the voltage signal $U(t)$ (averaged 512 times for the fiber-optic hydrophone and 64 times for the other two hydrophones) was recorded at each single point. The scanning distance was 50 mm for axial scans and 30 mm for radial scans. The scanning time was $\sim$90 min for an axial scan and $\sim$60 min for a radial scan, so the overall measuring time per measurement unit was between 4 and 5 h. The oxygen content after a measurement unit was typically < 5 mg/l. Each recorded waveform $U(t)$ was transformed to the frequency domain. The resulting voltage spectra $U(f)$ were lowpass-filtered with a third-order Butterworth filter (cutoff frequency: 20 MHz for the HNA-0400, 40 MHz for the membrane hydrophone, and 100 MHz for the fiber-optic probe) and then deconvolved using a linear interpolation of the frequency response data. For the HNA-0400, where no phase information on the frequency response was available, the phase was assumed to be constant across the whole frequency range: In other words, the deconvolution is only correcting for the variation in amplitude response in this case. The resulting pressure spectra $p(f)$ were then transformed back to the time domain to obtain the transient pressure waveforms $p(t)$.

Concerning the experimental procedure, three important things should be noted: First, although no absolute measurement of the exact distance from the transducer rim to the assumed focal position was performed, the maximum positions z_{max} found in all cases fitted quite well to the simple relation $z_{max} = c_S \Delta t_{foc}$, where $\Delta t_{foc} = z_{foc}/c_S$ is the time-of-flight of the signal as measured by an oscilloscope. In particular, no significant differences could be found in the maximum position between the different power levels. Second, the alignment of the axial translation direction (z axis) with the beam axis was tested for each hydrophone by finding (x_{max}, y_{max}) for two different z planes. If x_{max} or y_{max} was found to differ significantly between the two z planes, the transducer was realigned. Third, due to the soaking time and the long measurement time, the gas content of the water significantly increased during the course of each measurement unit. Hence, cavitation appeared in some cases and it could be heard by a faint ringing—the consequences can be seen in some of the results.

III. RESULTS

A. Fiber-optic displacement sensor

The fiber-optic displacement sensor was the only probe that withstood all investigated transducer/power level combinations without obvious problems. Under different conditions, destruction of the probe due to cavitation has been observed as well.[16] Hence, a partial erosion of the titanium layer during the measurements cannot be completely excluded. However, it can be assumed that such an erosion would have only a negligible influence on the frequency response. Typical waveforms (measured voltage waveform as well as the corresponding deconvolved pressure waveform) are shown in Fig. 2(a). Although the voltage waveform shows significant ripples, which are presumably due to the peak in the frequency response at $\sim$23 MHz, the deconvolution has obviously accounted well for that effect in this case, as the shape of the deconvolved waveform fits well to the modeled one. The noise equivalent pressure was determined as the standard deviation of a deconvolved signal in a part of the time domain where no HIFU signal was present (the same procedure applies to the other two hydrophones). It was found to be $\sim$300 kPa, which is slightly more than was observed before.[16]

In Fig. 2(b), the axial and radial peak pressure profiles are shown for all four transducer/power level combinations. In each case, the three scan directions indicate consistent behavior. All radial scan profiles show good symmetry and several side lobes can be found in each radial scan (only a few are shown in the diagrams).

For the SU-101 transducer, where the HIFU-Simulator is supposed to be valid, a good agreement between the simulations and the measurements can be observed for the higher power level, whereas the agreement is significantly worse for the lower power level. The same applies to the H-108MRA transducer. It is an unexpected finding that the agreement for the lower power levels is better than for the higher power levels, where nonlinear effects become more important. However, for a detailed study of this finding, measurements and simulations at more power levels would be required.

B. ONDA HNA-0400

The measurements with the ONDA HNA-0400 in the sound field of the H-108MRA transducer at 25 W show good

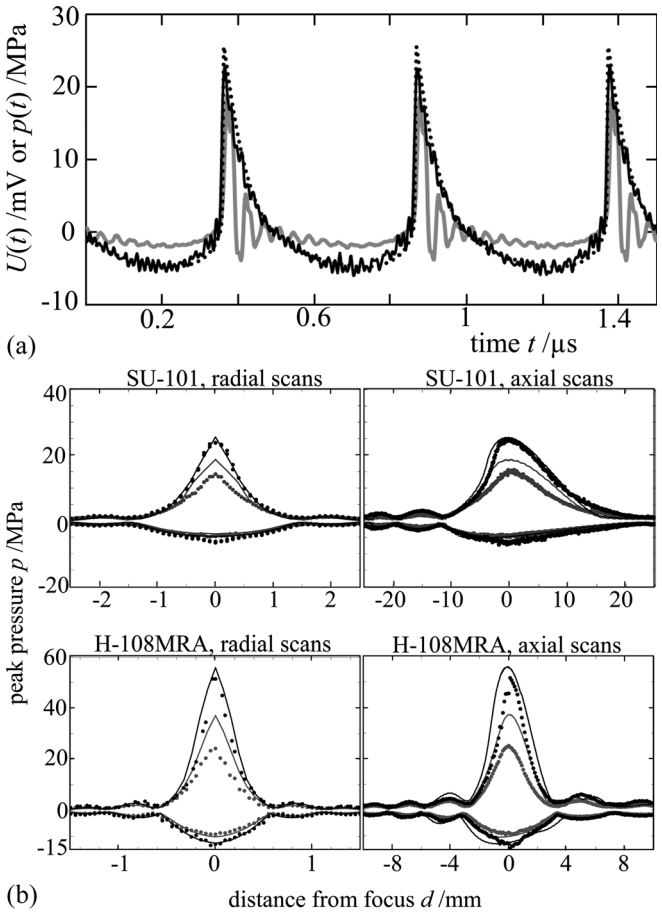

FIG. 2. (a) Waveforms within the focus of a SU-101 at an acoustical power level of 50 W, as measured with the fiber-optic displacement sensor. Measured voltage waveform (gray) and deconvolved pressure waveform (black), as well as pressure waveform from the HIFU-Simulator (dotted line) are shown. (b) Radial and axial peak pressure scans through the focus of the SU-101 and the H-108MRA transducer at acoustical power levels of 25 W (gray) and 50 W (black) as measured with the fiber-optic displacement sensor (points). The radial scans comprise results from two different scan directions perpendicular to each other (x and y—not distinguished by different symbols). For comparison, results from the HIFU-Simulator are also shown (lines).

agreement with the simulation outside the focal region and also with the peak-rarefactional pressure within the focal region; the peak-compressional pressure, however, is very different within the focal region. As can be seen in Fig. 3(a), especially the compressional pressure does not show such a steep rise as in the modeled waveforms. This might be due either to the large sensing element and the limited frequency range or to the phase response of the hydrophone, which was not available from the manufacturer. These assumptions will be further discussed in Sec. IV. The noise equivalent pressure of this probe was found to be ~130 kPa. During the z-scan in the field of the H-108MRA transducer at 50 W [see Fig. 3(b)], the measured amplitudes significantly decreased, which is likely due to damage to the HNA-0400. Nonetheless, measurements were also performed afterward in the field of the SU-101 transducer. However, these measurements should not be considered to be reliable results, as indicated by the strong ripples on the waveforms in the upper diagram of Fig. 3(a), which are believed to be a deconvolution artifact caused by a changed frequency response due to a (partial) damage of the sensor.

C. Coated membrane hydrophone

Some example waveforms from the measurements with the coated membrane hydrophone are given in Fig. 4(a), and the scan profiles in Fig. 4(b). The measurements in the field of the SU-101 transducer went smoothly and the results are in quite good agreement with those from the fiber-optic probe [compare Figs. 2(a) and 4(a)]. During the last scan in the field of the H-108MRA transducer at 25 W, the voltage signal disappeared more or less completely [see dotted gray line in Fig. 4(a, bottom)]. It seems likely that cavitation

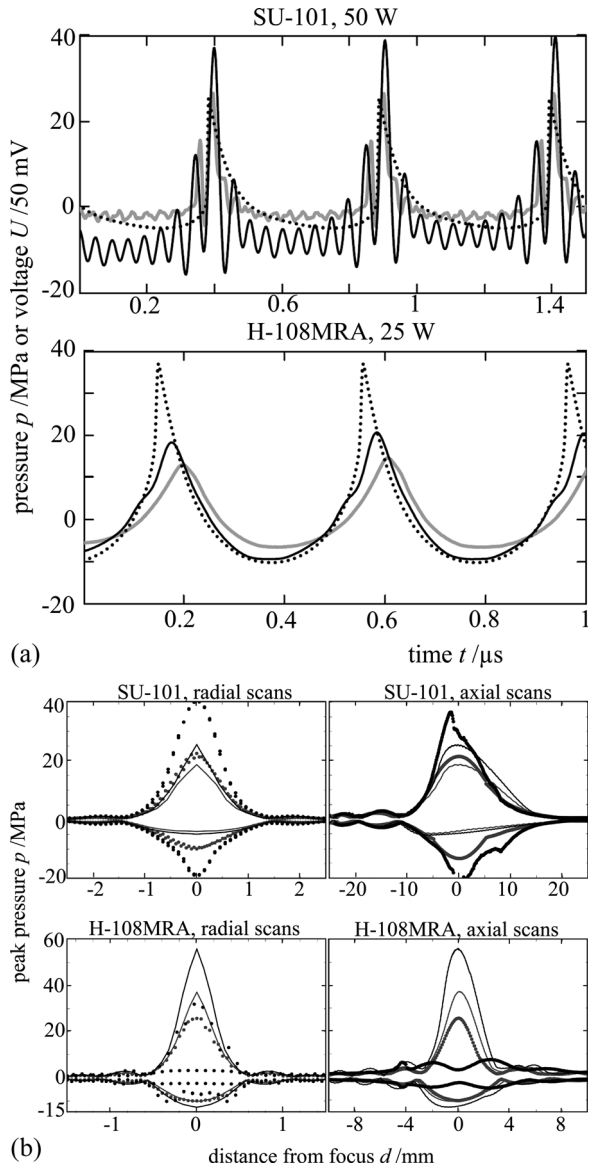

FIG. 3. (a) Waveforms within the focus of the SU-101 (top) and the H-108MRA (bottom) transducer at acoustical power levels of 50 and 25 W, respectively, as measured with the ONDA HNA400 needle hydrophone. Measured voltage waveforms (gray) and deconvolved pressure waveforms (black), as well as pressure waveforms from the HIFU-Simulator (dotted line) are shown. (b) Radial and axial peak pressure scans through the focus of the SU-101 and the H-108MRA transducer at acoustical power levels of 25 W (gray) and 50 W (black) as measured with the ONDA HNA400 needle hydrophone (points). The radial scans comprise results from two different scan directions perpendicular to each other (x and y—not distinguished by different symbols). For comparison, results from the HIFU-Simulator are also shown (lines).

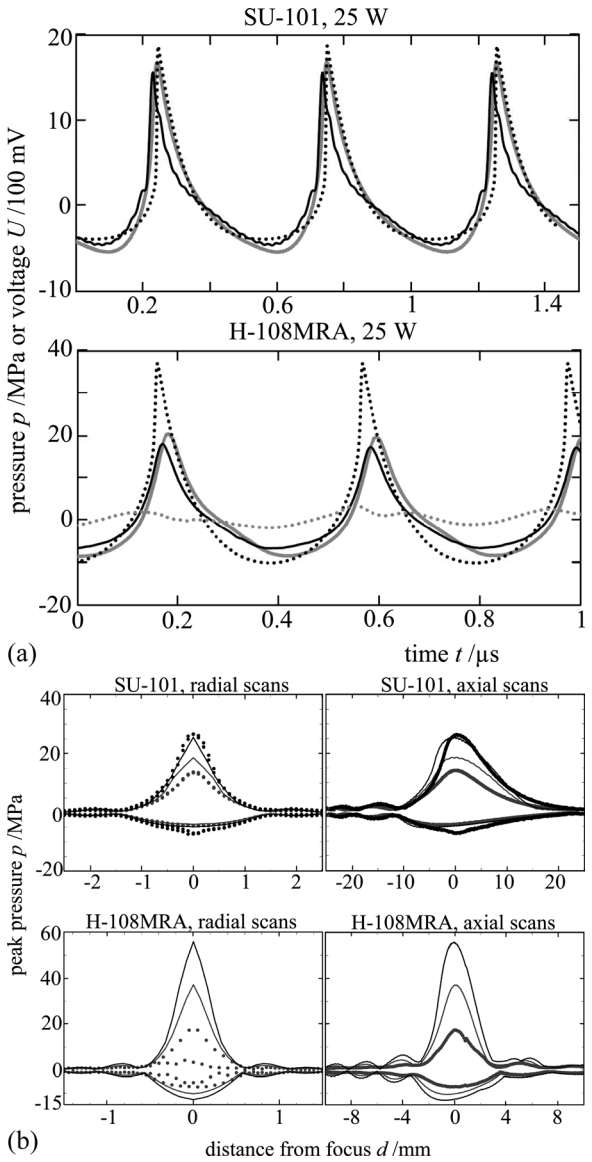

FIG. 4. (a) Waveforms within the focus of the SU-101 (top) and the H-108MRA (bottom) transducer at an acoustical power level of 25 W, as measured with the coated membrane hydrophone. Measured voltage waveforms (gray) and deconvolved pressure waveforms (black), as well as pressure waveforms from the HIFU-Simulator (dotted line) are shown. The dotted gray line shows the voltage of a measurement, where the hydrophone obviously was completely damaged. (b) Radial and axial peak pressure scans through the focus of the SU-101 and the H-108MRA transducer at acoustical power levels of 25 W (gray) and 50 W (black), as measured with the coated membrane hydrophone (points). The radial scans comprise results from two different scan directions perpendicular to each other (x and y—not distinguished by different symbols). For comparison, results from the HIFU-Simulator are also shown (lines).

eroded the electrodes. However, it cannot completely be excluded that the coating was gradually eroded during the preceding measurements, which would have changed the transfer characteristics. The noise equivalent pressure of the coated membrane hydrophone was found to be ~20 kPa.

IV. DISCUSSION

A. Comparison of measurements

In Table III, the peak compressional and rarefactional pressure values, as well as the −6 dB radii of focal regions from the different measurements and the simulations, are summarized. As peak values might be due to extreme outliers in the measured wave bursts, the spatial-peak temporal-average derived intensities I_{SPTA} are given additionally, which were calculated as

$$I_{\mathrm{SPTA}} = \frac{1}{t_2 - t_1} \cdot \int_{t_1}^{t_2} \frac{(p(t))^2}{\rho \cdot c_S} dt. \tag{3}$$

The integration region was chosen to start after the fifth cycle of each burst to exclude transient effects and $t_2 = t_1 + 10/f_0$ for averaging over ten cycles. Two of the three hydrophones did not withstand all of the investigated transducer/power level combinations; hence a direct comparison of all three hydrophones is hardly possible, especially as gradual changes in the hydrophones' frequency responses during the measurements cannot be ruled out. Nevertheless, some general observations can be made.

The results from the fiber-optic probe and the coated membrane hydrophone are in fairly good agreement, except for one measurement, where the coating of the membrane hydrophone may already have been partly eroded (H-108MRA, 25 W). For the other two measurements, the differences are smaller than the typical uncertainties of the calibration of ~15%, if the peak pressure values are considered. The same applies if one compares the measurements from the fiber-optic probe with those from the HNA-0400 for the measurement unit (SU-101, 25 W). For the intensity values, however, the differences are somewhat larger. It is a striking result of the measurements that discrepancies in the peak intensities of up to 50% were derived from the different devices. In particular, as the intensity is the relevant parameter for treatment planning, further work on standardization and safety issues is obviously needed.

Another distinct finding is, that the HIFU-Simulator predicts, except for one case, significantly higher peak compressional pressure values than was found from the measurements. Some possible explanations for this will be discussed in the following subsections.

B. Robustness

One striking outcome of the present work is the fact that two of the three hydrophones did not withstand the investigated sound fields. Concerning the commercial HIFU hydrophone, the HNA-0400, it should be noted that the data sheet supplied by the manufacturer states that the hydrophone is stress-tested "at the focus of a 1.5 MHz source, operated at 50% duty cycle in de-ionized, degassed water at 23 °C. This provides an exposure intensity of 715 W cm^{-2} temporal-average and 1430 W cm^{-2} pulse-average, corresponding to 15 MPa peak compressional and 3.7 MPa rarefactional pressure."[38] So the hydrophone has been exposed in this study to pressures outside the range of the stress test (compare values in Table III).

As the damage to hydrophones typically is predominantly due to mechanical forces and cavitation effects, there are two possible ways to overcome this problem. Either the robustness of the hydrophones has to be further improved or cavitation

TABLE III. Peak pressure values p_c, p_r (MPa), radii of −6 dB decay $r_{-6\,\mathrm{dB}}$ (mm), and spatial-peak temporal-average intensities I_{SPTA} (kW cm^{-2}) as derived from the different measurements and the simulation. Boldface typeface denotes unreliable/impossible measurements and italic typeface denotes simulations under nonvalid conditions and a measurement during which a probe broke.

	SU-101								H-108MRA							
	25 W				50 W				25 W				50 W			
	p_c	p_r	$r_{-6\,\mathrm{dB}}$	I_{SPTA}	p_c	p_r	$r_{-6\,\mathrm{dB}}$	I_{SPTA}	p_c	p_r	$r_{-6\,\mathrm{dB}}$	I_{SPTA}	p_c	p_r	$r_{-6\,\mathrm{dB}}$	I_{SPTA}
Fiber-optic setup	14.3	4.8	0.50	1.3	23.8	6.6	0.44	2.7	24.2	9.1	0.22	4.9	51.5	13.4	0.17	13.0
HNA-0400	…	…	…	…	…	…	…	…	25.8	9.8	0.26	5.1	…	…	…	…
Coated membrane	13.9	4.4	0.49	1.4	26.7	7.3	0.41	4.4	*17.4*	*7.2*	*0.26*	*3.0*	…	…	…	…
HIFU-Simulator	18.7	3.9	0.48	2.0	25.6	4.8	0.41	3.2	*37.3*	*10.1*	*0.21*	*9.1*	*55.6*	*12.6*	*0.21*	*17.6*

has to be avoided during measurements. The first approach has the drawback that mechanical stabilization or protection presumably goes along with a decrease in the acoustical performance. For the second approach, several suggestions have been reported to reduce or to avoid cavitation.[39] As one example, the use of an alternative liquid medium with a higher cavitation threshold has been suggested. However, measurements in any medium other than water may require a specific hydrophone calibration in this medium. Another way to avoid or at least impede cavitation is to continuously degas the water or to apply static pressure, which in turn requires additional technical modifications of typical setups.

However, the presence of any sensor is likely to reduce the cavitation threshold because of constructive acoustic interference close to the sensor and because the surface of the sensor provides a site for cavitation nuclei like very small bubbles to grow more easily. Thus, a more promising attempt might be to apply completely noninvasive[19–21] measurement techniques to the characterization of strong HIFU fields, which might also allow for measurements of pressure or intensity *in vitro*. However, some of these methods require tomographic reconstruction and the calibration of these methods remains a challenging task.

C. Filtering bandwidth

The results from the HIFU-Simulator can be found in the figures of the preceding subsections. It is within the nature of simulations that they do not necessarily reflect reality—for example, due to invalid assumptions of the model or due to an idealization of the (typically nonideal) real conditions. Therefore, it would not be advisable to take the results here as reference. However, the numerical simulation of the different sound fields allows the generation of data with a virtually unlimited frequency bandwidth, without noise and without spatial averaging, which is impossible for any real measurement. Hence, for a comparison between the simulations and the measurements and for an investigation into the significance of the mentioned effects, it is useful to study the effect of introducing bandwidth restrictions into the computational results. In Fig. 5, the results of calculative bandwidth limitations are shown, which were derived by filtering the modeled focal pressure waveforms [see Figs. 2(a), 3(a), and 4(a)] with a third-order Butterworth filter and different cutoff frequencies in the frequency domain. As predominantly higher frequency components are responsible for the sharpness of the positive waveform peaks, the peak compressional pressure values significantly decrease with decreasing bandwidth. As a notable result, the use of a hydrophone with a usable bandwidth of 20 MHz might lead to an underestimation of the peak compressional pressure of ∼15%. For the peak rarefactional pressure values the effect was much smaller than 1% for all considered cases (only one curve shown in Fig. 5). These findings are consistent with those in Sec. IV A and with calculations that predict errors in the measurement of rarefactional pressure to be rather due to lower limitations of the usable frequency range.[40] For the temporal-average intensities, an effect smaller than for the compressional pressure values was found.

D. Spatial averaging

Another point that has to be taken into account is the fact that the sensing hydrophone element has finite lateral dimensions, which consequentially means that every measurement represents a spatial averaging over the respective area. To investigate the significance of this effect, the peak compressional pressure distributions derived from the KZK model were averaged over circles with different radii around the focus. Such calculations yielded an underestimation of up to 30% for the peak compressional pressure in the worst

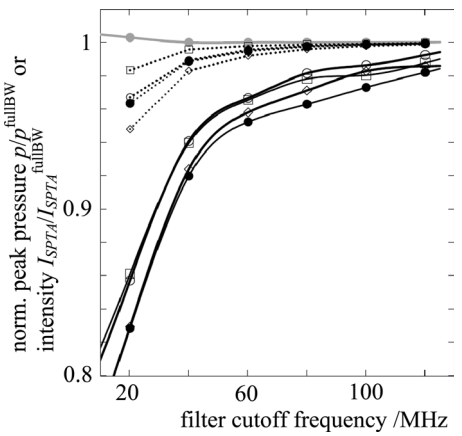

FIG. 5. Normalized pressure and intensity values at the focus as derived from the HIFU-Simulator and filtering with different −3 dB cutoff frequencies. ○: SU-101, 25 W; ◇: SU-101, 50 W; □: H-108MRA, 25 W; •: H-108MRA, 50 W. Full black lines: Normalized peak compressional pressure; gray line: Normalized peak rarefactional pressure; dotted lines: Normalized spatial-peak temporal-average intensities.

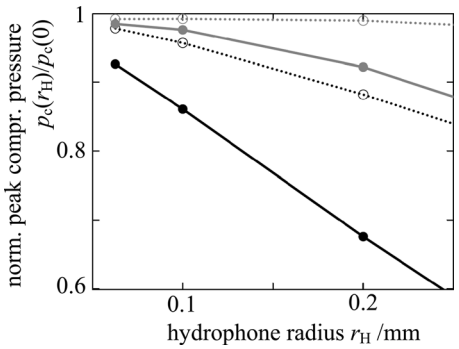

FIG. 6. Normalized compressional (black) and rarefactional (gray) peak pressure values at the focus as derived from the HIFU-Simulator and spatial averaging over different hydrophone radii. Dotted line: SU-101, full line: H-108MRA transducer. Points denote the nominal radii of the employed three hydrophones.

case (see Fig. 6), although again only a slight effect on the peak rarefactional pressure was found. The effect for the temporal-average intensities (not shown) was found to be almost the same as for the peak compressional values. However, for an exact analysis of this finding, an averaging of the deconvolved temporal pressure waveforms over the effective diameter (instead of the nominal diameter) would be required.

The commonly used, rather universal criterion for the maximum suitable effective radius r_H of a hydrophone for ultrasonic fields is[41]

$$r_H \leq \frac{\lambda}{8\,a_{\mathrm{act}}}\left(z_{\mathrm{foc}}^2 + a_{\mathrm{act}}^2\right)^{1/2}, \tag{4}$$

which means $r_H \leq 0.31$ mm for the SU-101 and $r_H \leq 0.15$ mm for the H-108MRA, if $\lambda = c_S/f_0$ is considered to be the relevant wavelength. In literature, theoretical and experimental investigations on the influence of the hydrophone diameter on measurements in nonlinearly distorted ultrasound fields at diagnostical power levels can be found.[42] However, no recommendations particularly for measurements in HIFU fields are available so far. The above-mentioned findings suggest that an even stricter criterion could be reasonable in strongly focused, nonlinearly distorted HIFU fields.

E. Deconvolution artifacts

In addition to the effects discussed in the preceding sections, the lack of any information about the phase of the frequency response for one of the three hydrophones is a possible error source. Again, the modeled waveforms can be used to demonstrate this effect. From the voltage measurement performed in the focus of the H-108MRA at 25 W with the ONDA HNA-0400 and the corresponding pressure spectrum from the numerical modeling, a complex frequency response can be obtained by dividing the former by the latter. For the harmonics of the fundamental frequency, the signal-to-noise ratio is high enough to obtain a reliable estimation of the phase information in this way. The resulting phase response for the HNA-0400 shows only a very weak frequency dependence for the first five harmonics of $\sim \pm 0.07$ rad. However, this estimation of the phase response is used to demonstrate the influence of the phase information on the deconvolution procedure. In Fig. 7, the waveform at the focus of the H-108MRA at 25 W as originally obtained from the numerical modeling (thick black line) is compared with signals that were convolved with the complex frequency response to imitate the influence of the hydrophone during a measurement and then were deconvolved with either the complex frequency response (gray line), the magnitude of the frequency response only (black line), or with the magnitude of the frequency response at the fundamental frequency only (dotted line). The same procedure was applied to the two other hydrophones and all spectra were filtered with a third-order Butterworth filter with $f_G = 20$ MHz to obtain comparable results. The difference between the thick black line and the gray line thus reflects the influence of the lowpass filtering. It is obvious that the coated membrane hydrophone reproduces the pressure waveform most faithfully for the latter two procedures because of the relatively small fluctuations in its frequency response. For the other two hydrophones, the necessity of applying an accurate deconvolution is considerably higher. However, except for the simple scaling attempt for the fiber-optic hydrophone the influence on the peak compressional and rarefactional pressure is rather small in the considered cases.

Another possible source for deconvolution artifacts are deviations of the real magnitude of the frequency response from the calibration data, which could be due to either a change in the frequency response during the time after the calibration or to uncertainties in the calibration. Such deviations could lead to noticeable under- or overestimations of certain frequency ranges. It is therefore a useful addition to

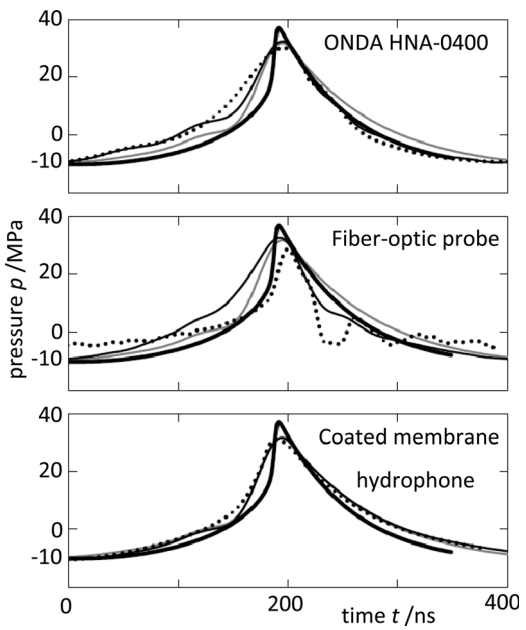

FIG. 7. Influence of the phase information on the deconvolved waveform. Results from numerical modeling (thick black line) have been convolved with each hydrophone's complex frequency response and then have been deconvolved, respectively, with either the complex frequency response (gray line), the magnitude of the frequency response only (black line) or with the magnitude of the frequency response at the fundamental frequency only (dotted line). Dotted line in the middle diagram has been multiplied with 0.5 to fit in the scale.

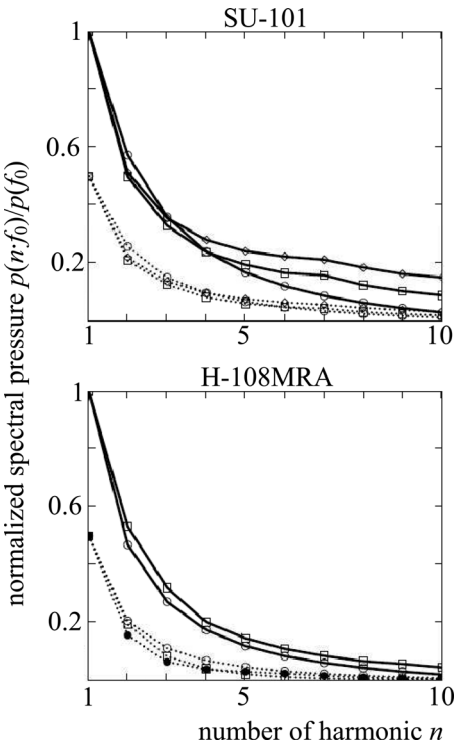

FIG. 8. Spectral pressure of the harmonics of the fundamental frequency at the focus. ○: HIFU-Simulator; ♢: Coated membrane hydrophone; □: Fiber-optic probe; •: ONDA HNA-0400. Dotted lines denote 25 W (scaled with 0.5), full lines 50 W. $n = 1$ denotes the fundamental frequency f_0.

the time domain considerations and the phase considerations to perform an additional analysis of the magnitude data in the frequency domain. In Fig. 8, the harmonic pressure components of the first ten harmonics are shown for all reliable measurements as well as for the modeled waveforms. The scaling to the first fundamental masks the absolute discrepancies, which for the fundamental are roughly up to 30% between simulations and measurements, and up to 15% between different measurements. Nevertheless, the normalized curves agree fairly well for the different methods and for both transducers, except for one case (SU-101, 50 W). On the one hand, this verifies the calibrated magnitude frequency responses of the different hydrophones and, on the other hand, it might be taken as a hint that the numerical modeling yields reliable results also for the nonvalid case of the H-108MRA transducer.

V. CONCLUSION

This paper has presented an evaluation of three different hydrophones used for measurements in the fields of two different HIFU transducers at 25 and 50 W. The comparison of the results from the measurements with each other and with a widely used numerical model clearly shows that the quantitative analysis of such fields remains a challenging task. Significant differences were observed that may be partly explained by different active diameters of the hydrophones and by different usable frequency ranges. Nevertheless, these discrepancies reflect the necessity for standardized recommendations for field measurements in HIFU fields, both in terms of the choice of measurement device and the analysis method.

Susceptibility to destruction by cavitation is a further problem. For the hydrophones studied, neither a metallic coating (ONDA HNA-0400) nor a polyurethane coating (membrane hydrophone) could protect the sensitive parts from destruction.

Noninvasive measurement methods could be a solution to this problem in the future, provided that they are capable of measuring the large and rapid pressure variations that can occur in HIFU fields and that the difficulties concerning issues like calibration and tomographic reconstruction are overcome.

ACKNOWLEDGMENTS

The present work was performed within the framework of the iMERA + project "JRP7 – External Beam Cancer Therapy," and financing by the European Union is gratefully acknowledged. Work at NPL was co-funded by the U.K. National Measurement System. The authors would also like to thank H.-P. Reimann (PTB) for the modification of the scanning setup and J. Soneson (FDA) for the permission to use the software package "HIFU-Simulator."

[1] G. ter Haar and C. Coussios, "High intensity focused ultrasound: Past, present and future," Int. J. Hyperthermia **23**, 85–87 (2007).
[2] G. ter Haar, "Acoustic surgery," Physics Today **54**, 29–34 (2001).
[3] A. Blana, B. Walter, S. Rogenhofer, and W. F. Wieland, "High-intensity focused ultrasound for the treatment of localized prostate cancer: 5-year experience," Urology **63**, 297–300 (2004).
[4] K. Rove, K. Sullivan, and E. Crawford, "High-intensity focused ultrasound: Ready for primetime," Urol. Clin. North Am. **37**, 27–35 (2010).
[5] G. ter Haar and C. Coussios, "High intensity focused ultrasound: Physical principles and devices," Int. J. Hypertherm. **23**, 89–104 (2007).
[6] N. McDannold, G. T. Clement, P. Black, F. Jolesz, and K. Hynynen, "Transcranial magnetic resonance imaging guided focused ultrasound surgery of brain tumors: Initial findings in 3 patients," Neurosurgery **66**, 323–332 (2010).
[7] S. Mitnovetski, A. Almeida, J. Goldstein, A. Pick, and J. Smith, "Epicardial high-intensity focused ultrasound cardiac ablation for surgical treatment of atrial fibrillation," Heart, Lung Circ. **18**, 28–31 (2009).
[8] D. Chen and J. Wu, "An *in vitro* feasibility study of controlled drug release from encapsulated nanometer liposomes using high intensity focused ultrasound," Ultrasonics **50**, 744–749 (2010).
[9] B. Liberman, D. Gianfelice, Y. Inbar, A. Beck, T. Rabin, N. Shabshin, G. Chander, S. Hengst, R. Pfeffer, A. Chechick, A. Hanannel, O. Dogadkin, and R. Catane, "Pain palliation in patients with bone metastases using MR-guided focused ultrasound surgery: A multicenter study," Ann. Surg. Oncol. **16**, 140–146 (2008).
[10] L. L. Xiong, J. H. Hwang, X. B. Huang, S. S. Yao, C. J. He, X. H. Ge, H. Y. Ge, and X. F. Wang, "Early clinical experience using high intensity focused ultrasound for palliation of inoperable pancreatic cancer," JOP **10**, 123–129 (2009).
[11] S. M. Howard and C. I. Zanelli, "HIFU transducer characterization using a robust needle hydrophone," in *Sixth International Symposium on Therapeutic Ultrasound*, edited by C. Coussios and G. ter Haar (AIP, New York, 2007), pp. 8–14.
[12] P. Morris, A. Hurrell, A. Shaw, E. Zhang, and P. Beard, "A Fabry–Pérot fiber-optic ultrasonic hydrophone for the simultaneous measurement of temperature and acoustic pressure," J. Acoust. Soc. Am. **125**, 3611–3622 (2009).
[13] J. E. Parsons, C. A. Cain, and J. B. Fowlkes, "Cost-effective assembly of a basic fiber-optic hydrophone for measurement of high-amplitude therapeutic ultrasound fields," J. Acoust. Soc. Am. **119**, 1432–1440 (2006).
[14] R. G. Minasamudram, P. Arora, G. Gandhi, A. S. Daryoush, M. A. El-Sherif, and P. A. Lewin, "Thin film metal coated fiber optic hydrophone probe," Appl. Opt. **48**, G77–G82 (2009).
[15] M. S. Canney, M. R. Bailey, L. A. Crum, V. A. Khoklova, and O. A. Sapozhnikov, "Acoustic characterization of high intensity focused ultrasound

fields: A combined measurement and modelling approach," J. Acoust. Soc. Am. **124**, 2406–2420 (2008).
[16]J. Haller, V. Wilkens, K.-V. Jenderka, and C. Koch, "Characterization of a fiber-optic displacement sensor for measurements in high-intensity focused ultrasound fields," J. Acoust. Soc. Am. **129**, 3676–3682 (2011).
[17]M. E. Schafer, J. Gessert, and W. Moore, "Development of a high intensity focused ultrasound (HIFU) hydrophone system," in *Fifth International Symposium on Therapeutic Ultrasound*, edited by G. T. Clement, N. J. McDonald, and K. Hynynen (AIP, New York, 2005), pp. 609–613.
[18]P. Kaczkowski, B. Cunitz, V. Khokhlova, and O. Sapozhnikov, "High resolution mapping of nonlinear MHz ultrasonic fields using a scanned scatterer," Proc.-IEEE Ultrason. Symp. **2003**, 982–985 (2003).
[19]M. Radicke, J. Mende, A.-L. Kofahl, J. Wild, D. Ulucay, B. Habenstein, M. Deimling, P. Trautner, B. Weber, and K. Maier, "Acoustic radiation contrast in MR images for breast cancer diagnostics—initial phantom study," Ultrasound Med. Biol. **37**, 253–261 (2011).
[20]P. Hariharan, M. R. Myers, R. A. Robinson, S. H. Maruvada, J. Sliwa, and R. K. Banerjee, "Characterization of high intensity focused ultrasound transducers using acoustic streaming," J. Acoust. Soc. Am. **123**, 1706–1719 (2008).
[21]C. I. Zanelli, S. DeMarta, C. W. Hennige, and M. M. Kadri, "Beamforming for therapy with high intensity focused ultrasound (HIFU) using quantitative schlieren," Proc.-IEEE Ultrason. Symp. **1993**, 1211–1214 (1993).
[22]J. E. Soneson, "A user-friendly software package for HIFU simulation," in *Eighth International Symposium on Therapeutic Ultrasound*, edited by E. S. Ebbini (AIP, New York, 2009), pp. 165–169.
[23]J. Hoffelner, H. Landes, M. Kaltenbacher, and R. Lerch, "Finite element simulation of nonlinear wave propagation in thermoviscous fluids including dissipation," IEEE Trans. Ultrason. Ferroelectr. Freq. Control **48**, 779–786 (2001).
[24]S. Behnia, A. Jafari, F. Ghalichi, and A. Bonabi, "Finite-element simulation of ultrasound brain surgery: Effects of frequency, focal pressure, and scanning path in bone-heating reduction," Cent. Eur. J. Phys. **6**, 211–222 (2008).
[25]Y. Nakajima, J. Uebayashi, Y. Tamura, and Y. Matsumoto, "Large-scale simulation for HIFU treatment to brain," in *26th International Symposium on Shock Waves*, edited by K. Hannemann and F. Seiler (Springer, Berlin, 2009), Vol. 2, pp. 863–868.
[26]F. Li, R. Feng, Q. Zhang, J. Bai, and Z. Wang, "Estimation of HIFU induced lesions *in vitro*: Numerical simulation and experiment," Ultrasonics **44**(Suppl. 1), e337–e340 (2006).
[27]M. F. Hamilton and C. L. Morfey, "Model equations," in *Nonlinear Acoustics*, edited by M. F. Hamilton and D. T. Blackstock (Academic, San Diego, 1998), Chap. 3, pp. 41–63.
[28]E. Filonenko and V. Khokhlova, "Effect of acoustic nonlinearity on heating of biological tissue by high-intensity focused ultrasound," Acoust. Phys. **47**, 541–549 (2001).
[29]V. Khokhlova, M. Bailey, J. Reed, B. Cunitz, P. Kaczkowski, and L. Crum, "Effects of nonlinear propagation, cavitation, and boiling in lesion formation by high intensity focused ultrasound in a gel phantom," J. Acoust. Soc. Am. **119**, 1834–1848 (2006).
[30]P. Meaney, M. Cahill, and G. ter Haar, "The intensity dependence of lesion position shift during focused ultrasound surgery," Ultrasound Med. Biol. **26**, 441–450 (2000).
[31]H.-M. Kramer, J.-M. Bordy, E. van Dijk, J. Dobrovodsky, S. Duane, G. Durando, R.-P. Kapsch, B. Karaböce, C. Koch, A. Kosunen, M. Pimpinella, and A. Shaw, "Metrology in external beam cancer therapy," in *Added Value Through Better Measurement: 14th International Metrology Congress* (Collège Français de Métrologie, Paris, 2009).
[32]V. Wilkens and C. Koch, "Amplitude and phase calibration of hydrophones up to 70 MHz using broadband pulse excitation and an optical reference hydrophone," J. Acoust. Soc. Am. **115**, 2892–2903 (2004).
[33]*IEC 62127-2: Ultrasonics–Hydrophones—Part 2: Calibration for Ultrasonic Fields up to 40 MHz, edition 1.0* (International Electrotechnical Commission, Geneva, 2007).
[34]V. Wilkens, S. Sonntag, and O. Bessonova, "Messung hochintensiver therapeutischer Ultraschallfelder (HITU) mit breitbandigen Membranhydrophonen (Measurement of high intensity therapeutic ultrasound (HITU) fields with broadband membrane hydrophones)," in *Fortschritte der Akustik—DAGA* 2011, 925–926 (2011).
[35]S. Meeks and R. Ting, "The evaluation of static and dynamic stress on the piezoelectric and dielectric properties of PVDF," J. Acoust. Soc. Am. **75**, 1010–1012 (1984).
[36]R. H. Tancrell, D. T. Wilson, and D. Ricketts, "Properties of PVDF polymer for sonar," Proc. IEEE Ultrason. Symp. **1985**, 624–629 (1985).
[37]B. Zeqiri and C. J. Bickley, "A new anechoic material for medical ultrasonic applications," Ultrasound Med. Biol. **26**, 481–485 (2000).
[38]ONDA Corporation, HNA-0400 data sheet, Sept. 2009.
[39]*IEC 61161: Ultrasonics—Power Measurement—Radiation Force Balances and Performance Requirements*, 2nd ed. (International Electrotechnical Commission, Geneva, 2006).
[40]G. R. Harris, "Pressure pulse distortion by hydrophones due to diminished low frequency response," IEEE Trans. Ultrason. Ferroelectr. Freq. Control **42**, 989–992 (1995).
[41]K. Beissner, "Maximum hydrophone size in ultrasound field measurements," Acustica **59**, 61–66 (1985).
[42]B. Zeqiri and A. D. Bond, "The influence of waveform distortion on hydrophone spatial-averaging corrections—Theory and measurement," J. Acoust. Soc. Am. **92**, 1809–1821 (1992).